

Catalytic oxidative desulphurization of pyrolytic oils to fuels over different waste derived carbon-based catalysts

*Original*

Catalytic oxidative desulphurization of pyrolytic oils to fuels over different waste derived carbon-based catalysts / Tamborrino, V.; Costamagna, G.; Bartoli, M.; Rovere, M.; Jagdale, P.; Lavagna, L.; Ginepro, M.; Tagliaferro, A.. - In: FUEL. - ISSN 0016-2361. - ELETTRONICO. - 296:(2021), p. 120693. [10.1016/j.fuel.2021.120693]

*Availability:*

This version is available at: 11583/2887794 since: 2021-05-21T11:20:48Z

*Publisher:*

Elsevier Ltd

*Published*

DOI:10.1016/j.fuel.2021.120693

*Terms of use:*

This article is made available under terms and conditions as specified in the corresponding bibliographic description in the repository

*Publisher copyright*

Elsevier postprint/Author's Accepted Manuscript

© 2021. This manuscript version is made available under the CC-BY-NC-ND 4.0 license  
<http://creativecommons.org/licenses/by-nc-nd/4.0/>. The final authenticated version is available online at:  
<http://dx.doi.org/10.1016/j.fuel.2021.120693>

(Article begins on next page)

# 1 **Catalytic oxidative desulphurization of pyrolytic oils to fuels over different waste** 2 **derived carbon-based catalysts**

3 *Valentina Tamborrino<sup>1</sup>, Giulia Costamagna<sup>2</sup>, Mattia Bartoli<sup>1,3\*</sup>, Massimo Rovere<sup>1,3</sup>, Pravin Jagdale<sup>4</sup>,*  
4 *Luca Lavagna<sup>1,3</sup>, Marco Ginepro<sup>2</sup>, Alberto Tagliaferro<sup>1,3</sup>*

5 <sup>1</sup>Department of Applied Science and Technology, Polytechnic of Turin, C.so Duca degli Abruzzi 24, Turin, 10129, Italy

6 <sup>2</sup>Department of Chemistry, University of Turin, Via Pietro Giuria, 5, Torino, 10125, Italy

7 <sup>3</sup>National Consortium for Materials Science and Technology (INSTM), Via G. Giusti 9, Florence, 50121, Italy

8 <sup>4</sup>Center for Sustainable Future, Italian Institute of Technology, Via Livorno 60, Turin, 10144, Italy

9 DOI: <https://doi.org/10.1016/j.fuel.2021.120693>

## 10 **Abstract**

11 In this work, we reported the conversion through carbothermal process of two catalysts produced by  
12 pyrolyzing exhausted coffee and waste tires. We tailored the surface with anchored iron nanoparticles  
13 through a facile carbothermal route and tested them for catalytic oxidative desulphurization of high  
14 sulphur content oil derived from tires pyrolysis. We studied their activity in a biphasic system under  
15 different conditions reaching a desulphurization of up to 60 % by using an oil with a sulphur  
16 concentration of up to 7139 ppm. The extensive characterization proved the reliability of those  
17 materials as promising catalysts for upgrading of sulphur rich drop-in fuels.

18 **Keywords:** biochar; drop-in fuel; tires; pyrolysis; biphasic catalysis

## 19 **1.Introduction**

20 Increased accountability of European Union with regards to environmental issues has represented a  
21 formidable driving force for the development of sustainable processes[1]. As a consequence, tires  
22 landfilling was forbidden with the European Council Directive 1999/31/CE due to its dangerous  
23 impact on the environment and human health[2, 3]. Furthermore, sustainable and circular economy  
24 principles have growth leading to the exploration of alternatives end-life tires processes[4].

25 The simpler methods are their use as inert filler for constructions[5, 6] and as road asphalt[7] or for  
26 the direct production of raw materials such as rubber[8-10] and textiles[11]. Alternatively,  
27 thermochemical routes are cost-effective approaches for end-life tires treatment avoiding the  
28 complexity of alternative management routes [12] such their conversion through pyrolytic  
29 techniques[13, 14].

30 Oil recovered from pyrolysis of tires is a very attractive product stream due to their composition that  
31 is very close to an engine fuel[15]. Nonetheless, their sulphur content is generally very high avoiding  
32 their for real field applications and requires an upgrading process to met the fuel regulation requires.

33 Among the all upgrading procedure, catalytic oxidative desulphurization[16] is very interesting for  
34 meeting the sulphur limits of common fuels [17] under the principles of green chemistry[18]. Plenty  
35 of different approached are described in literature based on transition metal-based catalysts (i.e.  
36 cobalt [19], tungsten [20] and manganese [21] or polyoxometalates [22]) using air [23, 24] or  
37 peroxides as oxidant agents [25-27], in homogenous or biphasic systems [28-31].

38 Iron-based catalysts are very promising due to their low cost price and to the ability to enhance  
39 oxidative power of oxygenated water [32] through Fenton mechanism [33].

40 This procedure achieved remarkably performances in the degradation of benzothiophene [34] and  
41 desulphurization of diesel-like fuels [35] by using nanostructured catalysts. Nonetheless, these  
42 systems were produced by using unfriendly procedures and lead to the merely deposition of the iron  
43 nanoparticles onto the support surface. Carbothermal route could represent a simple and facile  
44 alternative to produce iron nanoparticles anchored onto carbon support through thermochemical  
45 conversion of iron salts to metal iron nanoparticles[36, 37].

46 In this study, we exploited the synergist effect of the use of waste-derived carbon support for the  
47 upgrading of waste-derived drop-in fuel. The integration of waste valorization and alternative fuels  
48 production could represent a first step for a deep re-think of sustainable platforms.

49 Here, we reported the development of two nanostructured iron-based catalysts produced though  
50 carbothermal conversion of exhausted coffee residues biochar (CC) and carbon recovered from the  
51 very same tire pyrolysis (TC). Nanostructured catalysts were used to upgraded oil from pyrolysis of  
52 tires though a biphasic catalytic desulphurization in a watery biphasic system.

53 The catalytic activity and catalyst structures were widely analyzed and compared achieving good  
54 results in desulphurization of high sulphur content oils. We also evaluated the effect of  
55 microstructured (CC) and nanostructured (TC) support in the catalytic performances.

## 56 **2. Materials and methods**

### 57 *2.1 Materials*

58 Fe (NO<sub>3</sub>)<sub>3</sub> nonahydrate EtOH (>98%), HNO<sub>3</sub> (65%) and H<sub>2</sub>O<sub>2</sub> (30% v/v) were purchased by Sigma  
59 Aldrich. Coffee powder was collected from Bar Katia (Turin, Italy) supplied by Vergnano (Arabica  
60 mixture). A Pirelli branched tire was used for this study.

## 61 2.2 Methods

### 62 2.2.1 Pyrolysis

63 Coffee was collected and dried at 105°C prior the pyrolytic process. Afterwards, 100 g were  
64 pyrolyzed using a vertical furnace and a quartz reactor, heating rate of 15 °C/min and kept at 800°C  
65 for 30 min accordingly with previous studies[38-41].

66 Tire was chopped in small pieces and pyrolyzed using a tubular furnace (Carbolite TZF 12/65/550) in  
67 nitrogen by using a heating rate of 15 °C/min and kept at 550°C for 30 min. Solid and liquid fractions  
68 were collected.

69 A thermogravimetric analysis (TGA) of the oil was performed from 25 to 900 °C using a TGA  
70 Mettler Toledo model 1600 in two different atmospheres (Argon and air) with a gas flux of 50 ml/min  
71 with a heating ramp of 10 °C/min to describe a possible oil composition.

### 72 2.2.3 Preparation and characterization of catalysts

73 Recovered carbon from tire and biochar produced by pyrolyzing exhausted coffee were used as  
74 starting materials for carbothermal process. 50 g of each of them were suspended in 250 mL of  
75 deionized water together with Fe(NO<sub>3</sub>)<sub>3</sub> (weight of Fe/ weight carbon precursor of 1:10). The solution  
76 was stirred for 10 min and dried in a ventilated oven at 105°C overnight. The dried materials were  
77 used without any additional purifications. Carbothermal process was run by using a tubular furnace  
78 (Carbolite TZF 12/65/550) in nitrogen atmosphere with a heating rate of 15 °C/min and kept at 800°C  
79 for 30 min. The solids recovered were analyzed prior and after carbothermal processes by using  
80 several techniques.

81 Morphology was studied by using a field emission scanning electron microscope (FESEM, Zeis  
82 SupraTM40, Oberkochen, Germany). The microscope was equipped with an energy dispersive X-ray  
83 detector (EDX, Oxford Inca Energy 450, Oberkochen, Germany) that was used to explore the  
84 elemental composition of catalysts.

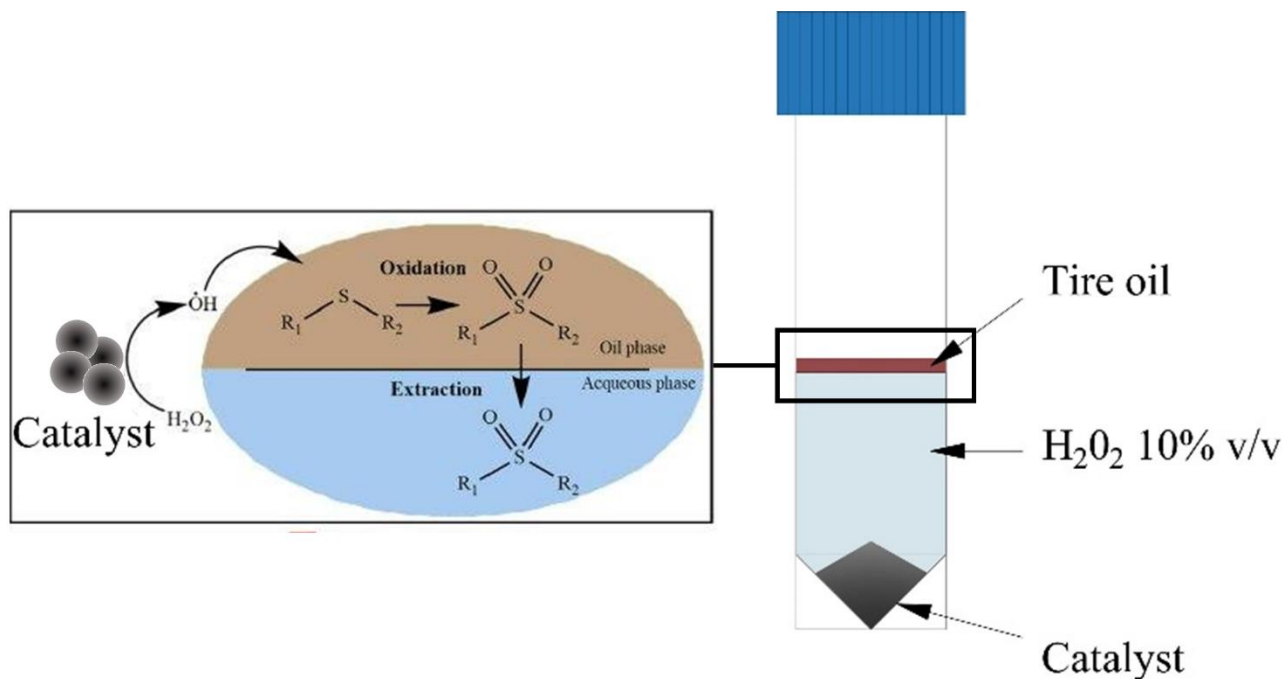
85 Raman spectra were collected by using Renishaw® Ramanscope InVia (H43662 model,  
86 Gloucestershire, UK). Signals were fitted according to methodology proposed by Tagliaferro et  
87 al.[42]

88 Surface of catalysts was investigated by using X-ray photoelectron spectroscopy (XPS). XPS  
89 spectrometer was a PHI 5000 Versaprobe Physical Electronics, Chanhassen, MN, USA) scanning X-  
90 ray photoelectron spectrometer (monochromatic Al K-alpha X-ray source with 1486.6 eV energy, 15  
91 kV voltage, and 1 mA anode current) to investigate surface chemical composition.

92 Specific surface area of the samples was measured by means of N<sub>2</sub> sorption at -196°C on a  
93 micrometrics Tristar II instrument (Micromeritics Instrument Corporation, USA). Brunauer–  
94 Emmett–Teller (BET) model was applied.

### 95 2.2.3 Catalysis

96 Catalytic tests were run in a biphasic systems as sketched in figure 1.



97

98

**Figure 1.** Scheme of catalytic set-up

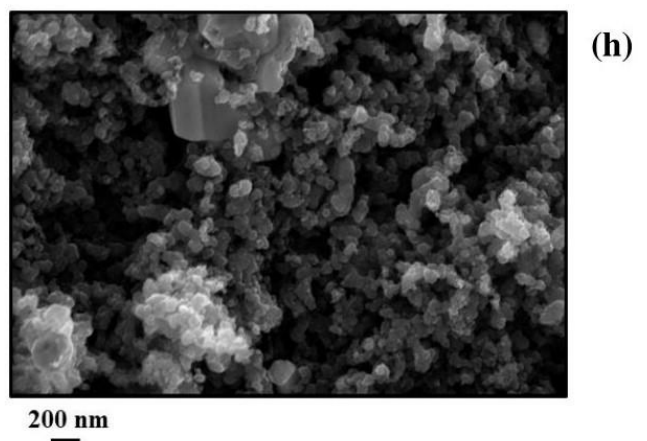
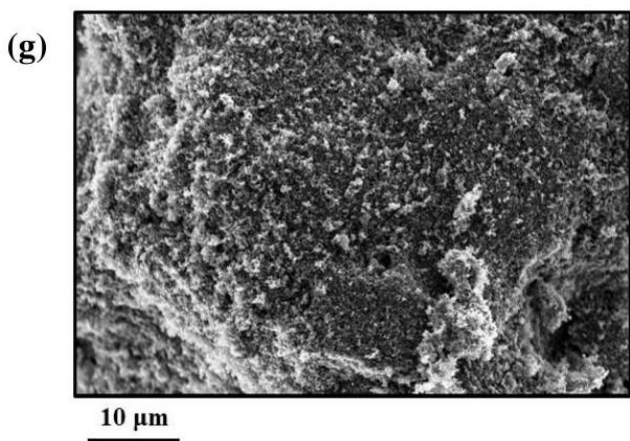
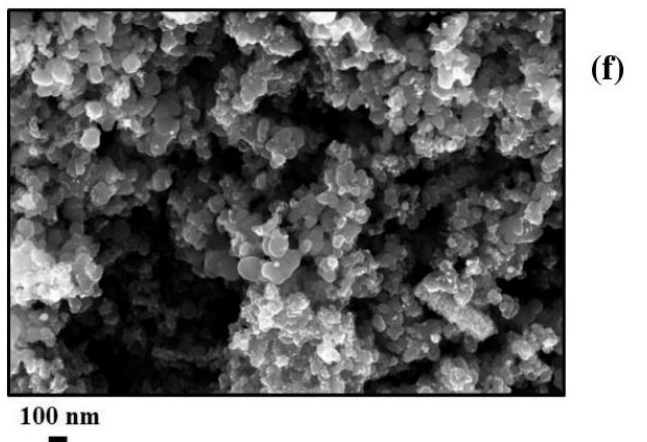
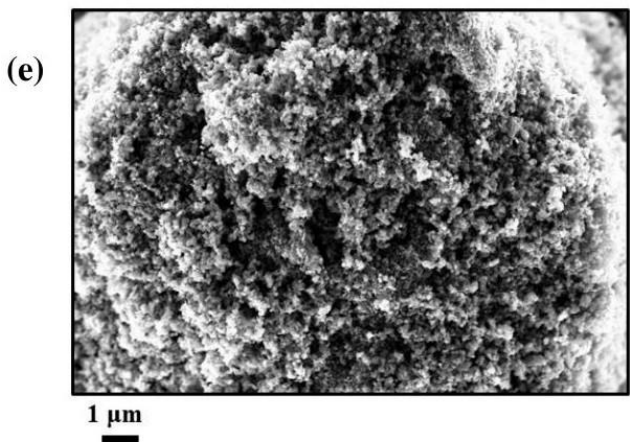
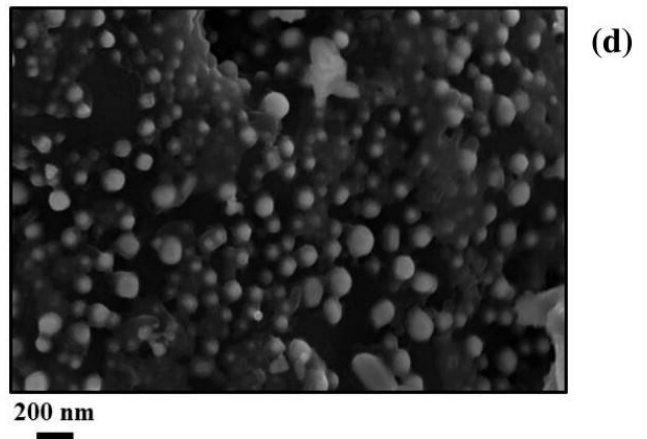
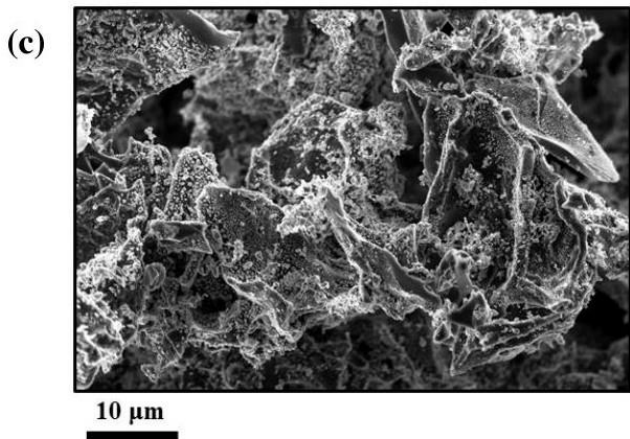
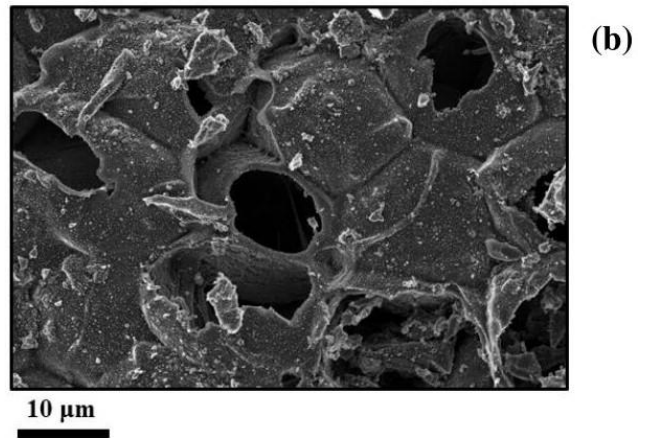
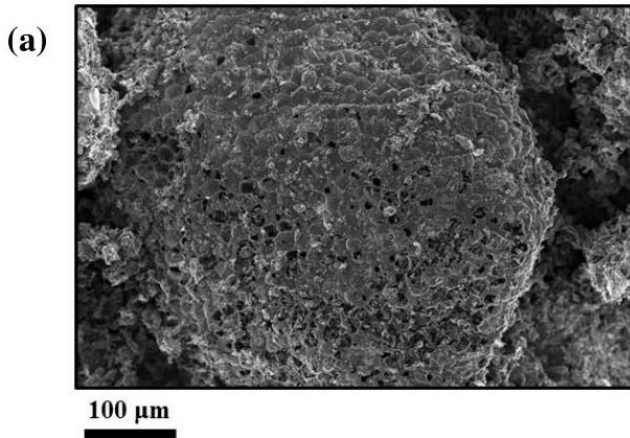
99 Catalysts were suspended in a 15 mL of a watery phase of H<sub>2</sub>O<sub>2</sub> (10 v/v%) and 2 g of oil recovered  
100 from pyrolysis of tires were added. The sealed vials were put in an oil bath at different temperatures  
101 (60, 80 and 100 °C), for different time (2, 4 and 6 h) and by using several catalysts loading. After the  
102 reaction, they were cooled down at room temperature and 10 mL of deionized water were added. Oily  
103 phases were collected and purified by suspended particles by using a centrifuge (1000 rpm for 10  
104 min). Recovered catalysts were collected, washed with acetone, dried at 105 °C overnight and further  
105 analyzed.

106 Sulphur concentration was determined by ICP (ICP-OES Perkin Elmer Optima 2000 DV) after acidic  
107 digestion in microwave oven (ETHOSUP Milestone) by using H<sub>2</sub>O<sub>2</sub> 30 v/v% in HNO<sub>3</sub> 65 wt.% (ratio  
108 1:9) with a power of 800W for 35 min.

109 **3. Results and discussion**

110 **3.1 Characterization of the catalysts**

111 Solid recovered from pyrolytic conversion of both exhausted coffee powder and waste tires were used  
112 as starting materials for carbothermal synthesis of catalysts[43, 44]. This facile approach has been  
113 used to tailor the surface of carbon from pyrolysis of exhausted coffee and waste tires with metal  
114 nanostructures as those shown in figure 2.



116 **Figure 2.** FESEM captions of a-b) biochar from exhausted coffee, c-d) CC prior catalysis, e-f)  
117 carbonized tires and g-h) TC prior catalysis

118 The surface of the coffee biochar prior carbothermal process (figure 2 a-b) was structured in  
119 micrometric sponge-like aggregates whose diameter is around 20 to 100  $\mu\text{m}$ . Coffee biochar shows a  
120 very low specific surface area of up to  $0.14 \text{ m}^2/\text{g}$  mainly due to the presence of micrometric pores  
121 formed during the release of volatile organic matters from the inner core of biomass particles.  
122 Contrary, carbon recovered from pyrolysis of tires showed a structure closely related to carbon black  
123 used for tires production[45]. This material was composed by of a complex agglomeration of carbon  
124 nanoparticles (similar to carbon black structure) with a specific surface area of up  $37.7 \text{ m}^2/\text{g}$ .  
125 Carbothermal synthesis of CC induces the formation on the carbonaceous surface of semispherical  
126 iron particles with diameters ranging from 50 to 150 nm (figure 2 c-d). CC surface area increased of  
127 up to  $46.2 \text{ m}^2/\text{g}$  due to the presence of nanoparticles together with the activation of carbon matrix, as  
128 described by Wang et al[46]. Similarly, TC displayed spherical iron nanoparticles anchored to carbon  
129 together with submicrometric iron aggregate (figure 2 h). TC showed a specific surface area  
130 increment of up to  $53.9 \text{ m}^2 / \text{g}$  mainly ascribed in this case to the presence of iron species. The more  
131 Comparing structures reported in figure 2d and figure 2 h, we observed that iron nanoparticles are  
132 fully exposed on surface of CC due the bigger size of carbon support compared with growing iron  
133 nanoparticles. Considering TC, carbon black particles were much smaller compared with iron  
134 nanoparticles and were unable to provide an anchoring surface as in the case of CC partially covering  
135 the nanostructures formed.

136 The elementary compositions of the CC, TC and their precursors were estimated by using EDX  
137 analysis as shown in Table 1.

138 **Table 1.** Elementary composition of pyrolyzed waste coffee obtained through EDX analysis,  $I_D/I_G$  and surface area before and after deposition of Fe  
 139 nanoparticles.

	Elemental analysis (wt.%)											$I_D/I_G$	Surface area ( $m^2/g$ )
	C	O	Mg	P	K	Ca	Fe	Si	S	Zn	Na		
<b>Coffee biochar</b>	86.9	8.9	0.6	0.5	1.8	1.3	Not detected	Not detected	Not detected	Not detected	Not detected	2.13	0.1
<b>Tires char</b>	91.9	4.8	Not detected	Not detected	Not detected	Not detected	Not detected	0.2	1.0	2.2	Not detected	2.04	37.7
<b>TC</b>	70.9	7.8	Not detected	Not detected	Not detected	1.5	19.8	0.5	1.3	1.5	Not detected	2.72 <sup>b</sup>	53.9
<b>TC<sup>a</sup></b>	72.8	4.4	Not detected	Not detected	Not detected	Not detected	21.1	0.2	0.5	Not detected	Not detected		52.1
<b>CC</b>	62.2	11.6	0.6	0.3	3.5	0.7	21.2	Not detected	Not detected	Not detected	Not detected	2.04 <sup>b</sup>	46.2
<b>CC<sup>a</sup></b>	60.5	15.8	0.7	1.1	1.2	0.7	19.5	Not detected	Not detected	Not detected	0.5		44.9

140 a) Catalysts after third catalytic cycle, b)  $I_D/I_G$  was unchanged before and after third catalytic cycle since the Raman spectra did not show any  
 141 appreciable differences

Coffee biochar showed an amount of carbon as carbon recovered from tires together with an appreciable amount of oxygen that could be associated to both residual group on carbon surface and to inorganic species. Inorganic species in coffee derived biochar derived from the biological fixation routes that originates the feedstock[47]. Additionally, carbon recovered from tires displayed a sulphur content of up to 0.5 wt.% due to the not complete conversion of sulphur into organic or volatile organic matters as previously described by Undri et al[48]. Furthermore, TC precursors showed a negligible native iron content estimated in less than 0.1 wt.% by analysis its ash content. After, carbothermal process TC showed a totally disappearing of sulphur due to its oxidation with formation of  $SO_x$ . The final [Fe] was attested in both cases around to 20 wt.% (19.8 wt.% and 21.2 wt.% for TC and CC respectively).

A further investigation of carbon structure of CC, TC and their precursors was run by using Raman spectroscopy as reported in figure 3.

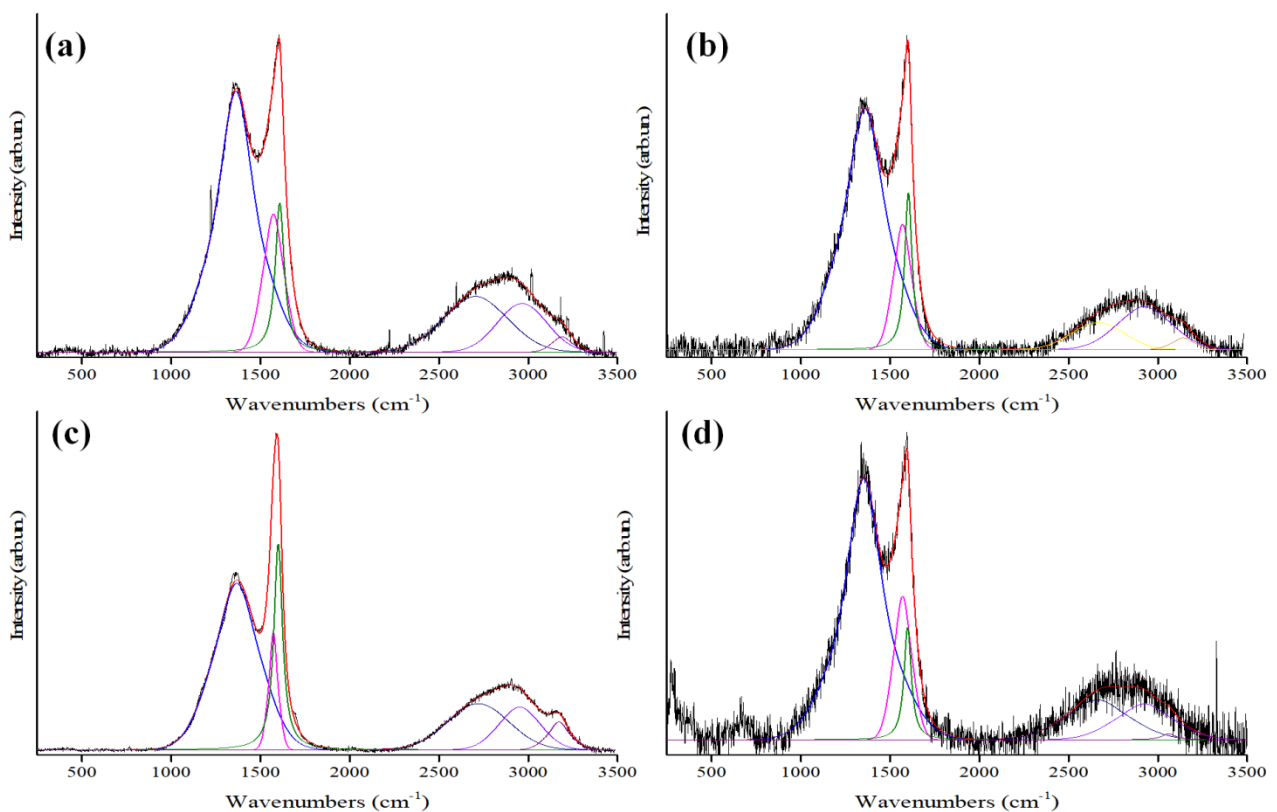


**Figure 3.** Raman spectra of a) biochar from exhausted coffee a coffee, b) CC prior catalysis, c) carbonized tires and d) TC prior catalysis. In black was reported the original Raman spectra and in red the fitted ones accordingly with the procedure proposed by Tagliaferro et al[42].

Raman spectroscopy is a powerfully tool to estimate the carbon degree of graphitization [49]. Particularly, the area ratio of D and G peaks in the region from 1300 to 1700  $\text{cm}^{-1}$  ( $I_D / I_G$ ) is possible investigated the carbonaceous structure disorder. Both coffee derived biochar and carbon recovered from waste tires were highly disordered materials with a  $I_D/I_G$  of up to 2.13 and 2.04 respectively[50]. After carbothermal process, CC and TC showed a decrement of  $I_D/I_G$  down to 2.04 while TC showed an increment of up to 2.72. This different behavior could be ascribed to the intrinsically differences between the two precursors. CC was produced by using a material that retained a relevant amount of residual functional groups and  $\text{sp}^3$  carbon content while carbon recovered from carbonization of tires was mainly composed by original carbon used to produce the neat tires. Considering CC, carbothermal process polished partially the carbon surface with a decrement of imperfections of carbonaceous structure while those are magnified for TC that was more ordered. This was also confirmed by the analysis of XPS spectra reported in the figure 4.

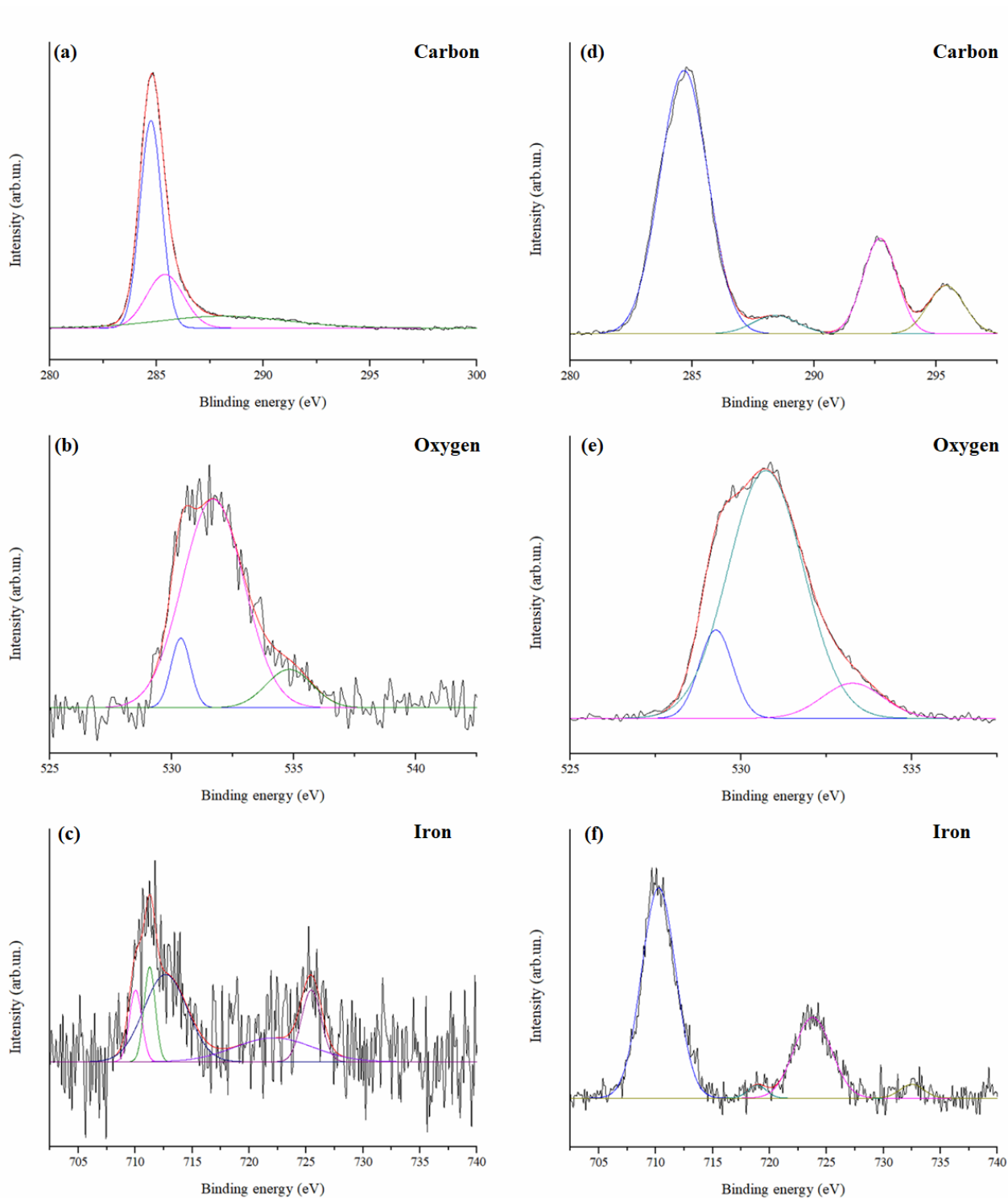


**Figure 4.** XPS spectra of CC (a-c) and TC (d-f). Carbon, oxygen and iron region are here displayed.

XPS spectra of CC (figure 4 a) showed a high amount of  $sp^2$  carbon preponderance (peak 284 eV) that reach the 68.5% of the total amount while  $sp^3$  represented only the 17.5 % (peak 284.9 eV). TC was composed by only  $sp^2$  carbon that was highly functionalized by oxygen functionalities proving the disorder increment observed by Raman spectroscopy. Those oxygen functionalities displayed peaks at 529, 531 and 533 eV. Peak at 531 eV represented up to 79% for both CC and TC and it was

associated with the presence of oxygen linked to quinoid carbons. The peak at 529.3 eV with a relative area of around 12 % was instead attributed to an oxygen bound to an iron in iron oxide[51]. Furthermore, the presence of Fe-OH residue on the particle surface was proved by the peak at 533.3 eV that represent the 8.9% of the total area[52]. The small area underlying this last peak shows that these groups exist only on the surface of the Fe nanoparticle and render the metal oxide layer partially defective. The formation of this defects could be ascribed to the presence of FeOOH formed during air passivation of iron nanoparticles as reported by Ponder et al.[53] at room temperature.[54]. Accordingly to figure 4 c and f, the spectrum of iron was shown and the presence of metallic iron and iron oxide across the peaks at 710.5 and 712.2 eV was detected. Iron oxidation state was in agreement with the peak at 530.0 eV of the oxygen spectrum, typical of a metal oxide. From the conclusions extrapolated from the carbon characterization before and after the carbothermic process, it was possible to obtain a model of the iron nanoparticle supported on a carbonaceous matrix. As can be seen from figure 5, the hypothesized iron nanoparticle model was based on a metallic iron core whose external surface was made by a layer of Fe<sub>2</sub>O<sub>3</sub> and FeOOH sites generated through passivation attached to the surface of the pyrolytic carbon through a very thin layer of iron carbide accordingly to Li et al[55]. CC showed a Fe(III)/Fe(0) ratio of 55.7% while TC showed a value of 53.3%.

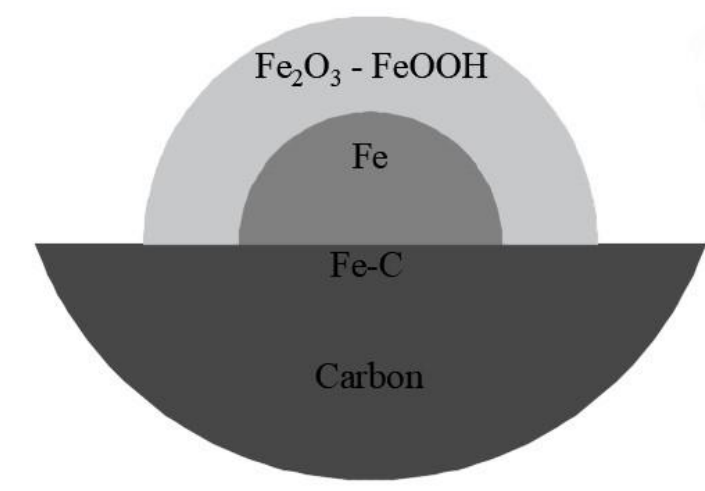


**Figure 5.** Hypothesized structure of iron particles anchored onto carbon support after carbothermal reduction and air passivation.

### 3.2 Preliminary considerations about oil recovered from pyrolysis of waste tires

Pyrolysis of waste tires was run at 550 °C accordingly with Ucar et al.[56] trying to maximizing the liquid yield. Nonetheless, the temperature adopted promoted the highest polycyclic sulphur aromatic compounds content as reported by Williams et al.[57]. In our study, oil recovered from the exhausted tires pyrolysis showed a concentration of up to 7139 ppm that greatly exceed the limit for use as drop-

in fuel. Nonetheless, the TGA profiles of oil shown in figure 6 confirmed a composition close to a conventional fuel, rich in C<sub>6</sub>-C<sub>10</sub> hydrocarbons, accordingly with the study reported by Kök et al.[58].

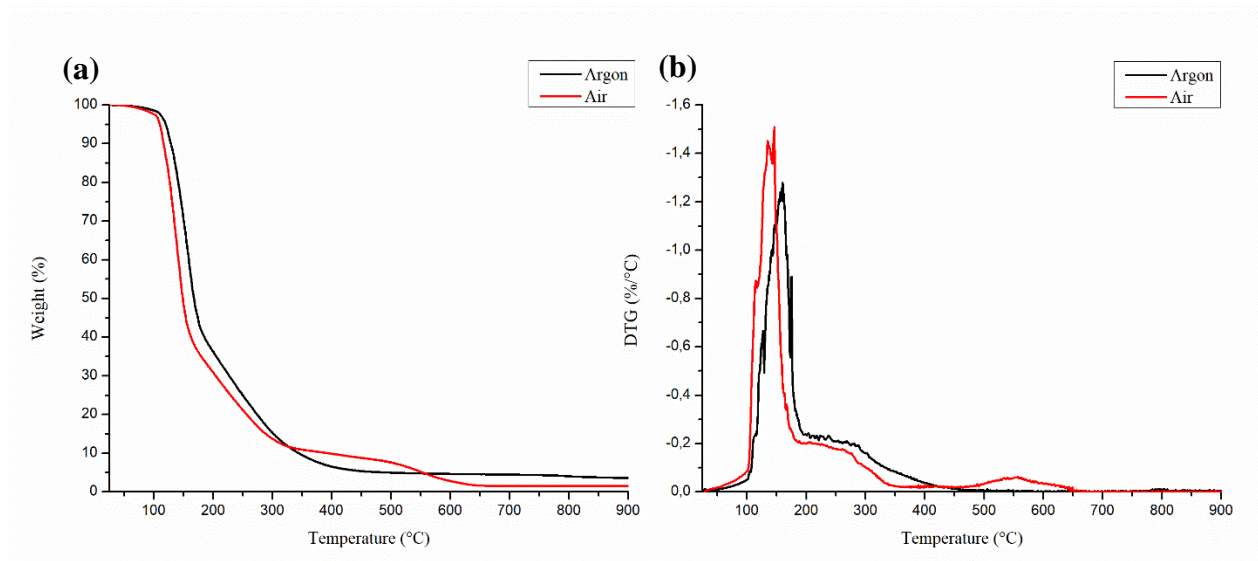


**Figure 6.** TGA and DTG of tire oil at Ar and air atmosphere from 25°C to 900°C.

Furthermore, the weigh losses between 500°C and 600°C could be attributed to the presence of polycyclic aromatic hydrocarbons which are more resistant to oxidation than other hydrocarbons.

### 3.3 Catalytic activity of CC and TC in oxidative desulphurization of oil recovered from pyrolysis of waste tires

Catalytic oxidative desulphurization of high sulphur content oil recovered from pyrolysis of tires was study by using CC and TC and varying several parameters as shown in table 2.

**Table 2:** Catalytic performances of CC and TC during oxidative desulphurization of high sulphur content oil recovered from pyrolysis of tires.

Entry	Catalyst	T (°C)	T (h)	Desulphurization <sup>(a)</sup> (%)	[S] (ppm)	Loading <sup>(b)</sup> (wt.%) / TON <sup>(c)</sup>
1	-	100	6	33.2	4769	-
2	CC	100	2	47.5	3747	5/219
3		100	4	52.3	3406	5/241
4		100	6	63.7	2592	5/293
5		60	6	36.4	4540	5/168
6		80	6	52.0	3425	5/240
7		100	6	49.0	3639	2/565

8		100	6	40.8	4223	10/94
9		100 <sup>(d)</sup>	6	39.2	3747	5/181
10		100	2	57.5	3036	5/283
11		100	4	58.1	2989	5/286
12		100	6	56.1	3132	5/276
13	TC	60	6	34.0	4709	5/167
14		80	6	36.1	4564	5/177
15		100	6	53.7	3305	2/660
16		100	6	52.2	3415	10/128
17		100 <sup>(d)</sup>	6	42.3	4116	5/169

(a) *Desulphurization* =  $100 - (100 * \text{final sulphur concentration} / \text{initial sulphur concentration})$ , (b) *loading* =  $100 * (\text{weight of iron} / \text{weight of oil})$ , (c) *TON* =  $\text{mmol of removed sulphur} / \text{mmol of accessible iron sites}$  (d) 3<sup>rd</sup> cycle of desulphurization.

Comparing the removal efficiencies of the catalysts and the H<sub>2</sub>O<sub>2</sub> (desulphurization of up to 33.2) under the same operating conditions (6h at 100 ° C with 5% g Fe / g oil) was evident the improvement induced by CC and TC that reached a desulphurization of up to 63.7 % and 53.7%. CC displayed the better performances compared with TC according to TON values. This was reasonably due to the effect of different carbon matrix. CC present iron nanoparticles fully exposed on the surface while TC was characterized by iron particles surrounded by nanometric carbon particles. Accordingly, TC activity could deplete by the hindrance of carbon matrix with lower iron nanoparticles accessibility.

By examining the entries 12, 13 and 14, an improvement in sulfur removal at high temperatures can be seen due to an evident kinetic boost. TC desulphurization rose from 36.1% at 80 ° C of up to 56.1% at 100 ° C. Similarly, temperature improved the CC desulphurization activity from 36.4% to 63.7% of. Temperature effect was scarcely influenced by the support but it was more related the activation energy together with phase transfer equilibria [59].

The catalyst loading is the other key parameter of the investigated. Catalyst loading of 2 % induced a reduction of desulphurization compared to the use of 5% for both CC and TC. Surprisingly, a catalyst loading of up to 10 wt.% lead to a decrement of desulphurization at 100°C after 6 h down to 40.8 % for CC while TC was unaffected. This was reasonably due to aggregation phenomena of micrometric particles of CC that did not occurred by using TC composed by nanometric carbon particles. Additionally, the original high sulphur content represented an obstacle to an efficient removal by using a biphasic approach with the extracted sulphone that rapidly reached the saturation of watery phase. Nonetheless, CC and TC displayed catalytic performances very close to systems

operating on tires derived oil[28, 60] even if none of previously published research based on biphasic systems treated oil with a sulphur content high such the one used in the present study.

Both CC and TC showed a reduction of activity after the third catalytic cycle down to 39.2% and 42.3% respectively. This was not related to iron leaching as proved by iron content retention as shown in table 2 but it was ascribed by a sized increment of iron particles as shown in figure 7.

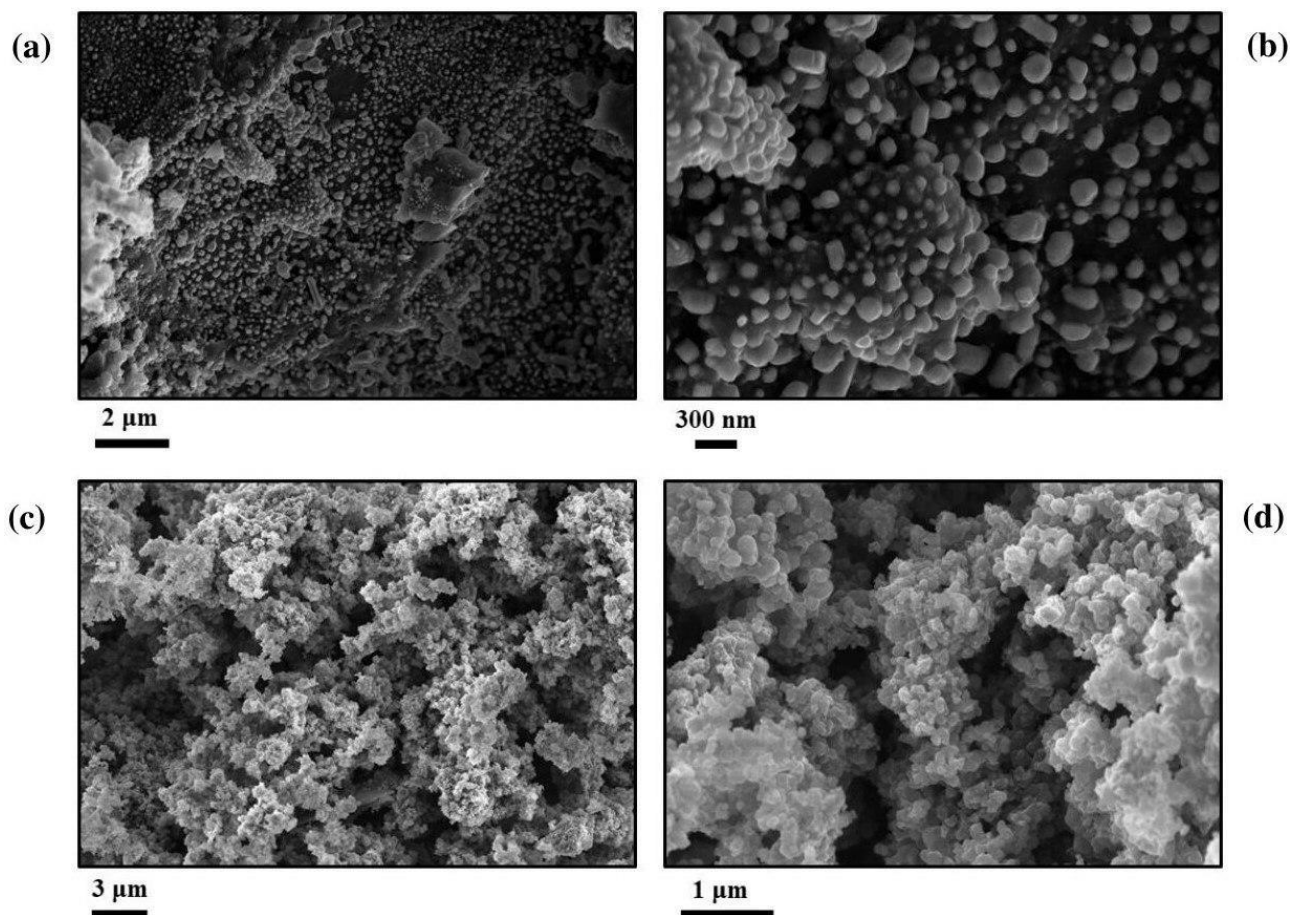


**Figure 7.** FESEM captions at different magnifications of CC (a-b) and TC (c-d) after three catalytic cycles.

CC showed an increment of particles average diameter of up to 100-300 nm while TC shows iron aggregated covered by spherical carbon nanoparticles.

However, the XPS spectra of recycled catalysts (figure 8) support the observed loss of reactivity due to the composition change on the catalyst surface.

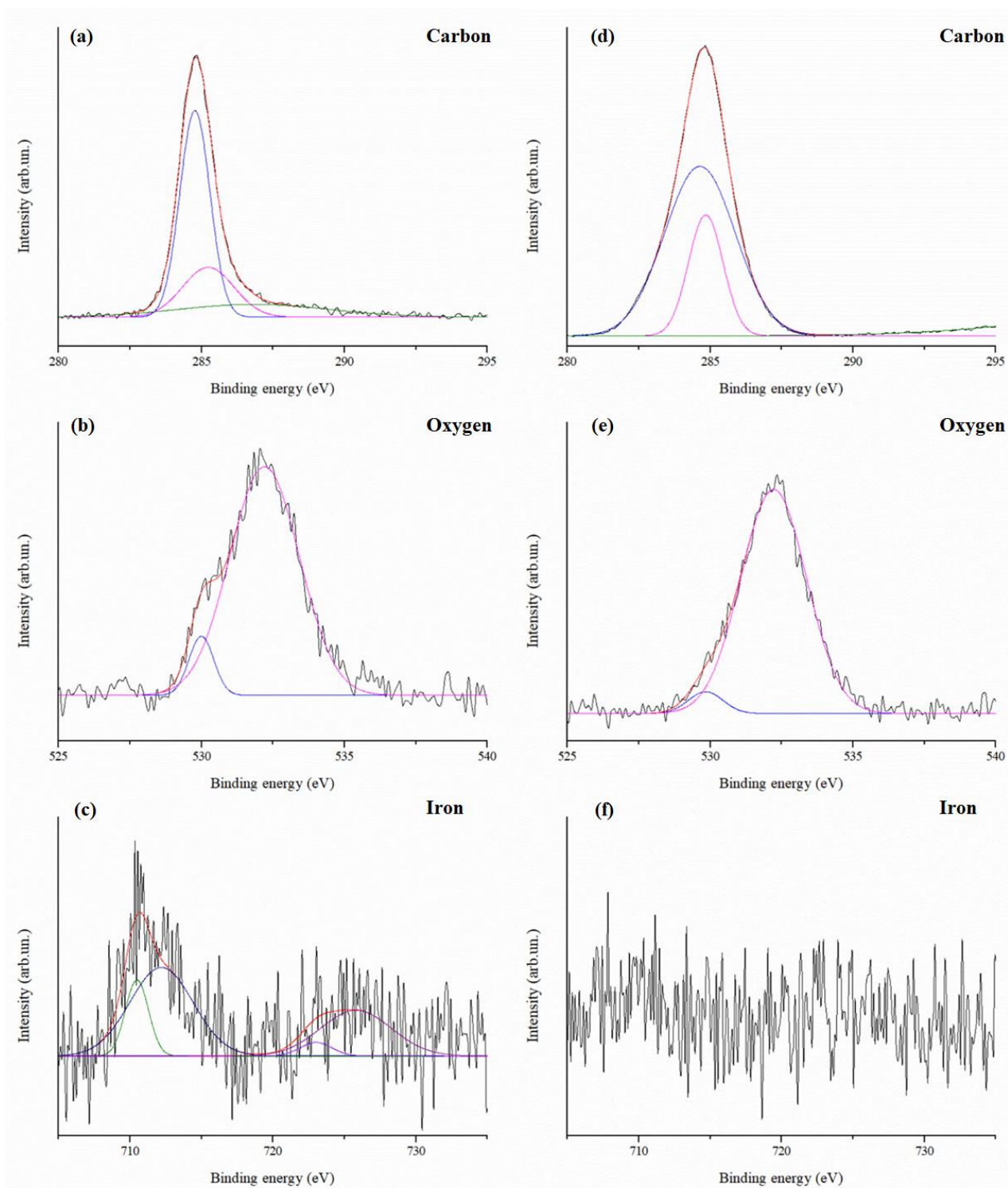


**Figure 8.** XPS spectra of CC (a-c) and TC (d-f) after the 3<sup>rd</sup> catalytic run. Carbon, oxygen and iron region are here displayed.

The loss of reactivity was also due to the increasing of the thickening of the crystal lattice of the iron oxide which reduces the tension on the same thus relaxing the orbitals. About each spectrum shown in figure 8, the iron signal of TC (figure 8 f) was characterized by a high noise level which did not

allow the detection of any peak. A fitting analysis of the iron spectrum of CC was performed although the large noise because of the micrometric size of the unpacked material from this type of catalyst. In particular, five peaks were distinct (the last two are replicas) while the three initial peaks are identifiable to a metallic iron, Fe-OH and iron oxide. About oxygen spectra, the position of the oxygen peaks has remained unchanged, so the catalyst continues to present oxides of iron and oxygen of a quinoidic nature. While the signal of carbon (figure 8 a), the spectrum of CC a showed the insertion of a new peak at 285.3 eV which is associated with the formation of a C-OH bond caused by the action of H<sub>2</sub>O<sub>2</sub>. The other two peaks at 284 and 288.1 eV of area, respectively, of 56.8 and 18.9% of the total, mark, as previously seen, the presence of C sp<sup>2</sup> and C of a quinoidic nature.

We supposed that the original structures of CC and TC underwent to different deactivation process as such reported in figure 9

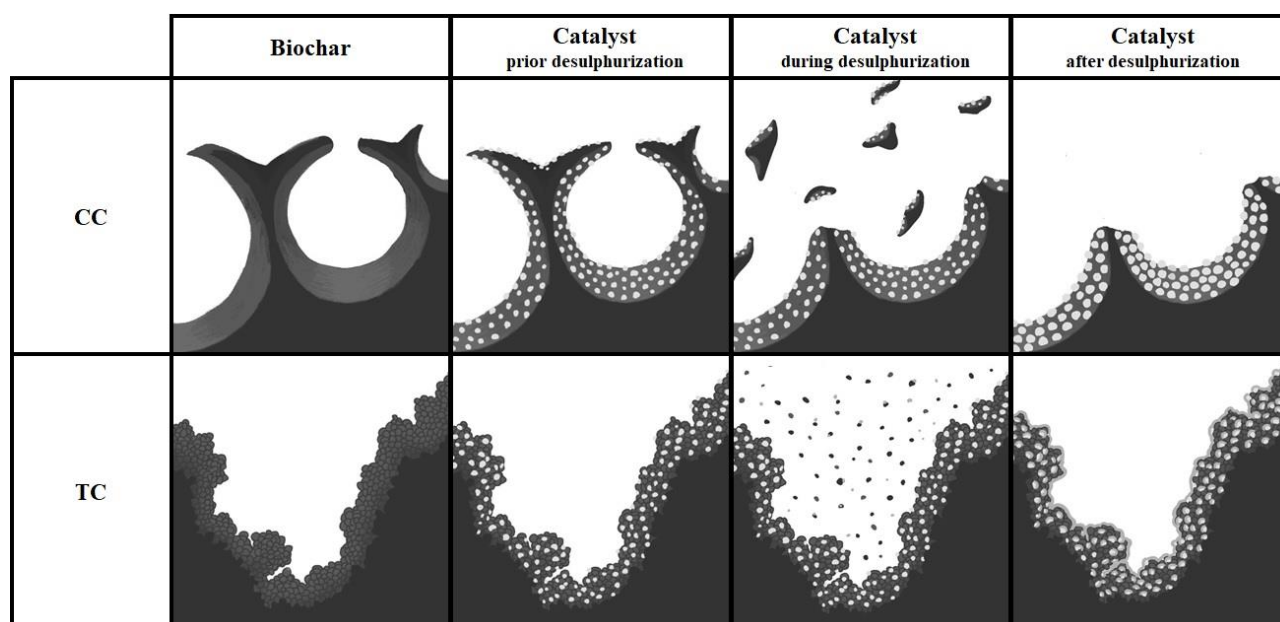


**Figure 9.** Evolution of the catalysts during the catalytic oxidative desulphurization of oil from tires pyrolysis.

According with FESEM analysis (figure 8 b), iron nanoparticles anchored onto CC increased their sized with a decrement of available catalytic sites on the surface. TC deactivation was mainly due to the covering of the iron nanoparticles by the spherical carbon particles of the support. This proved lower anchoring of iron nanostructures to TC than CC. The surface flatterring of CC was caused by the unpacking of micrometric carbon particles so modifying the surface morphology, as shown in figure 7 a.

#### **4. Conclusions**

In this work we reported the production and catalytic desulphurization of high sulphur content oil recovered from pyrolysis of tires by using biphasic catalytic oxidative desulphurization. Catalytic systems proposed were based on conversion of two waste streams through a facile carbothermal process capable to produce highly active heterogeneous catalysts characterized by nanostructured iron-based material. Air passivation after the carbothermal processes was a key step for achieving a hemispherical external layer of  $\text{Fe}_2\text{O}_3$  and  $\text{FeOOH}$  on an iron-based core. Thanks to the special geometry of the catalytic system created, CC showed a desulphurization ability of up to over 60% by using high sulphur content oil at the best conditions (at  $100^\circ\text{C}$  with a residence time of 6 hours). The morphological characteristics of the pyrolyzed waste streams were fundamental to describe the behavior of the catalytic system during the desulfurization processes. TC was successful in maintaining constant the desulphurization rate at different conditions thanks to submicrometric structure which increases the phase transfer between the reactants in the biphasic system. While the CC shows a micrometric structure, covered by nanometric iron-based particles, which tends to influence more the kinetics of the catalytic system. Despite this, iron-based materials produced by carbothermic processes could be considered a great improvement in Fenton reactions for oxidative desulphurization thanks to easier separation through magnetic proprieties and absence of leaching into reaction solution.

#### **References**

- [1] Leiserowitz AA, Kates RW, Parris TM. Sustainability values, attitudes, and behaviors: A review of multinational and global trends. *Annu Rev Environ Resour* 2006;31:413-44.
- [2] Nadal M, Rovira J, Díaz-Ferrero J, Schuhmacher M, Domingo JL. Human exposure to environmental pollutants after a tire landfill fire in Spain: Health risks. *Environment international* 2016;97:37-44.
- [3] Singh A, Spak SN, Stone EA, Downard J, Bullard RL, Pooley M, et al. Uncontrolled combustion of shredded tires in a landfill—Part 2: Population exposure, public health response, and an air quality index for urban fires. *Atmospheric Environment* 2015;104:273-83.

- [4] Lavagna L, Nisticò R, Sarasso M, Pavese M. An analytical mini-review on the compression strength of rubberized concrete as a function of the amount of recycled tires crumb rubber. *Materials* 2020;13(5):1234.
- [5] Záleská M, Pavlík Z, Čítek D, Jankovský O, Pavlíková M. Eco-friendly concrete with scrap-tyre-rubber-based aggregate—Properties and thermal stability. *Construction and Building Materials* 2019;225:709-22.
- [6] Gupta T, Siddique S, Sharma RK, Chaudhary S. Behaviour of waste rubber powder and hybrid rubber concrete in aggressive environment. *Construction and Building Materials* 2019;217:283-91.
- [7] Lo Presti D. Recycled Tyre Rubber Modified Bitumens for road asphalt mixtures: A literature review. *Construction and Building Materials* 2013;49:863-81.
- [8] Quadrini F, Santo L, Musacchi E. A sustainable molding process for new rubber products from tire recycling. *Progress in Rubber, Plastics and Recycling Technology* 2019;35(1):41-55.
- [9] Schmidt M, Spieth H, Haubach C, Kühne C. Rubber mats made from recycled used tyres. 100 *Pioneers in Efficient Resource Management*. Springer; 2019, p. 222-5.
- [10] Sunthonpagasit N, Duffey MR. Scrap tires to crumb rubber: feasibility analysis for processing facilities. *Resources, Conservation and Recycling* 2004;40(4):281-99.
- [11] Banaszkiwicz K, Badura M. Experimental investigation on the application of recycled tires polymer fibers as a BTEX removal material. *SN Applied Sciences* 2019;1(6):558.
- [12] Labaki M, Jeguirim M. Thermochemical conversion of waste tyres—a review. *Environ Sci Pollut Res* 2017;24(11):9962-92.
- [13] Martínez JD, Puy N, Murillo R, García T, Navarro MV, Mastral AM. Waste tyre pyrolysis—A review. *Renewable and Sustainable Energy Reviews* 2013;23:179-213.
- [14] Sathiskumar C, Karthikeyan S. Recycling of waste tires and its energy storage application of by-products—a review. *Sustainable Materials and Technologies* 2019:e00125.

- [15] Kyari M, Cunliffe A, Williams PT. Characterization of oils, gases, and char in relation to the pyrolysis of different brands of scrap automotive tires. *Energy & Fuels* 2005;19(3):1165-73.
- [16] Rajendran A, Cui T-y, Fan H-x, Yang Z-f, Feng J, Li W-y. A comprehensive review on oxidative desulfurization catalysts targeting clean energy and environment. *Journal of Materials Chemistry A* 2020;8(5):2246-85.
- [17] Iruretagoyena D, Montesano R. Selective Sulfur Removal from Liquid Fuels Using Nanostructured Adsorbents. *Nanotechnology in Oil and Gas Industries*. Springer; 2018, p. 133-50.
- [18] Anastas P, Eghbali N. Green chemistry: principles and practice. *Chemical Society Reviews* 2010;39(1):301-12.
- [19] Murata S, Murata K, Kiden K, Nomura M. A novel oxidative desulfurization system for diesel fuels with molecular oxygen in the presence of cobalt catalysts and aldehydes. *Energy & Fuels* 2004;18(1):116-21.
- [20] Yan X-M, Mei P, Lei J, Mi Y, Xiong L, Guo L. Synthesis and characterization of mesoporous phosphotungstic acid/TiO<sub>2</sub> nanocomposite as a novel oxidative desulfurization catalyst. *Journal of Molecular Catalysis A: Chemical* 2009;304(1):52-7.
- [21] Sampanthar JT, Xiao H, Dou J, Nah TY, Rong X, Kwan WP. A novel oxidative desulfurization process to remove refractory sulfur compounds from diesel fuel. *Applied Catalysis B: Environmental* 2006;63(1):85-93.
- [22] Trakarnpruk W, Rujiraworawut K. Oxidative desulfurization of gas oil by polyoxometalates catalysts. *Fuel Processing Technology* 2009;90(3):411-4.
- [23] Lü H, Gao J, Jiang Z, Yang Y, Song B, Li C. Oxidative desulfurization of dibenzothiophene with molecular oxygen using emulsion catalysis. *Chemical communications* 2007(2):150-2.
- [24] Zhang W, Zhang H, Xiao J, Zhao Z, Yu M, Li Z. Carbon nanotube catalysts for oxidative desulfurization of a model diesel fuel using molecular oxygen. *Green Chemistry* 2014;16(1):211-20.

- [25] Collins FM, Lucy AR, Sharp C. Oxidative desulphurisation of oils via hydrogen peroxide and heteropolyanion catalysis. *Journal of Molecular Catalysis A: Chemical* 1997;117(1-3):397-403.
- [26] Wang D, Qian EW, Amano H, Okata K, Ishihara A, Kabe T. Oxidative desulfurization of fuel oil: Part I. Oxidation of dibenzothiophenes using tert-butyl hydroperoxide. *Applied Catalysis A: General* 2003;253(1):91-9.
- [27] Zhu W, Li H, Gu Q, Wu P, Zhu G, Yan Y, et al. Kinetics and mechanism for oxidative desulfurization of fuels catalyzed by peroxo-molybdenum amino acid complexes in water-immiscible ionic liquids. *Journal of Molecular Catalysis A: Chemical* 2011;336(1):16-22.
- [28] Haw K-G, Bakar WAWA, Ali R, Chong J-F, Kadir AAA. Catalytic oxidative desulfurization of diesel utilizing hydrogen peroxide and functionalized-activated carbon in a biphasic diesel-acetonitrile system. *Fuel Processing Technology* 2010;91(9):1105-12.
- [29] Zhang M, Zhu W, Xun S, Li H, Gu Q, Zhao Z, et al. Deep oxidative desulfurization of dibenzothiophene with POM-based hybrid materials in ionic liquids. *Chemical engineering journal* 2013;220:328-36.
- [30] Li C, Jiang Z, Gao J, Yang Y, Wang S, Tian F, et al. Ultra-Deep Desulfurization of Diesel: Oxidation with a Recoverable Catalyst Assembled in Emulsion. *Chemistry-A European Journal* 2004;10(9):2277-80.
- [31] Zhang Q, Zhu M, Jones I, Zhang Z, Zhang D. Desulfurization of Spent Tire Pyrolysis Oil and Its Distillate via Combined Catalytic Oxidation using H<sub>2</sub>O<sub>2</sub> with Formic Acid and Selective Adsorption over Al<sub>2</sub>O<sub>3</sub>. *Energy & Fuels* 2020;34(5):6209-19.
- [32] Neyens E, Baeyens J. A review of classic Fenton's peroxidation as an advanced oxidation technique. *Journal of Hazardous materials* 2003;98(1):33-50.
- [33] Barb W, Baxendale J, George P, Hargrave K. Reactions of ferrous and ferric ions with hydrogen peroxide. *Nature* 1949;163(4148):692-4.

- [34] Zhang J, Wang G, Zhang L, Fu X, Liu Y. Catalytic oxidative desulfurization of benzothiophene with hydrogen peroxide catalyzed by Fenton-like catalysts. *Reaction Kinetics, Mechanisms and Catalysis* 2014;113(2):347-60.
- [35] Flores R, Rodas A, Gasperin R. Oxidative desulfurization of diesel fuel oil using supported Fenton catalysts and assisted with ultrasonic energy. *Petroleum Science* 2019;16(5):1176-84.
- [36] Shen Y. Carbothermal synthesis of metal-functionalized nanostructures for energy and environmental applications. *Journal of Materials Chemistry A* 2015;3(25):13114-88.
- [37] Hoch LB, Mack EJ, Hydutsky BW, Hershman JM, Skluzacek JM, Mallouk TE. Carbothermal synthesis of carbon-supported nanoscale zero-valent iron particles for the remediation of hexavalent chromium. *Environmental science & technology* 2008;42(7):2600-5.
- [38] Arrigo R, Bartoli M, Malucelli G. Poly (lactic Acid)–Biochar Biocomposites: Effect of Processing and Filler Content on Rheological, Thermal, and Mechanical Properties. *Polymers* 2020;12(4):892.
- [39] Arrigo R, Jagdale P, Bartoli M, Tagliaferro A, Malucelli G. Structure–Property Relationships in Polyethylene-Based Composites Filled with Biochar Derived from Waste Coffee Grounds. *Polymers* 2019;11(8):13.
- [40] Giorcelli M, Bartoli M. Development of Coffee Biochar Filler for the Production of Electrical Conductive Reinforced Plastic. *Polymers* 2019;11(12):17.
- [41] Strongone V, Bartoli M, Jagdale P, Arrigo R, Tagliaferro A, Malucelli G. Preparation and Characterization of UV-LED Curable Acrylic Films Containing Biochar and/or Multiwalled Carbon Nanotubes: Effect of the Filler Loading on the Rheological, Thermal and Optical Properties. *Polymers* 2020;12(4).
- [42] Tagliaferro A, Rovere M, Padovano E, Bartoli M, Giorcelli M. Introducing the Novel Mixed Gaussian-Lorentzian Lineshape in the Analysis of the Raman Signal of Biochar. *Nanomaterials* 2020;10(9):1748.

- [43] Thompson E, Danks A, Bourgeois L, Schnepf Z. Iron-catalyzed graphitization of biomass. *Green Chemistry* 2015;17(1):551-6.
- [44] Bartoli M, Giorcelli M, Jagdale P, Rovere M, Tagliaferro A. A Review of Non-Soil Biochar Applications. *Materials* 2020;13(2):291-6.
- [45] Gómez-Hernández R, Panecatí-Bernal Y, Méndez-Rojas MÁ. High yield and simple one-step production of carbon black nanoparticles from waste tires. *Heliyon* 2019;5(7):e02139.
- [46] Wang Y, Xia Q, Bai X, Ge Z, Yang Q, Yin C, et al. Carbothermal activation synthesis of 3D porous g-C<sub>3</sub>N<sub>4</sub>/carbon nanosheets composite with superior performance for CO<sub>2</sub> photoreduction. *Applied Catalysis B: Environmental* 2018;239:196-203.
- [47] Grembecka M, Malinowska E, Szefer P. Differentiation of market coffee and its infusions in view of their mineral composition. *Science of the Total Environment* 2007;383(1-3):59-69.
- [48] Undri A, Sacchi B, Cantisani E, Toccafondi N, Rosi L, Frediani M, et al. Carbon from microwave assisted pyrolysis of waste tires. *Journal of Analytical and Applied Pyrolysis* 2013;104:396-404.
- [49] Ferrari AC, Robertson J. Interpretation of Raman spectra of disordered and amorphous carbon. *Physical review B* 2000;61(20):14095.
- [50] Guizani C, Haddad K, Limousy L, Jeguirim M. New insights on the structural evolution of biomass char upon pyrolysis as revealed by the Raman spectroscopy and elemental analysis. *Carbon* 2017;119:519-21.
- [51] Yamashita T, Hayes P. Analysis of XPS spectra of Fe<sup>2+</sup> and Fe<sup>3+</sup> ions in oxide materials. *Applied surface science* 2008;254(8):2441-9.
- [52] McIntyre N, Zetaruk D, Owen D. X-Ray photoelectron studies of the aqueous oxidation of Inconel-600 alloy. *Journal of the Electrochemical Society* 1979;126(5):750.
- [53] Ponder SM, Darab JG, Bucher J, Caulder D, Craig I, Davis L, et al. Surface chemistry and electrochemistry of supported zerovalent iron nanoparticles in the remediation of aqueous metal contaminants. *Chemistry of Materials* 2001;13(2):479-86.

- [54] Fung K, Qin B, Zhang X. Passivation of  $\alpha$ -Fe nanoparticle by epitaxial  $\gamma$ -Fe<sub>2</sub>O<sub>3</sub> shell. *Materials Science and Engineering: A* 2000;286(1):135-8.
- [55] Li J, Lan H, Liu H, Zhang G, An X, Liu R, et al. Intercalation of Nanosized Fe<sub>3</sub>C in Iron/Carbon To Construct Multifunctional Interface with Reduction, Catalysis, Corrosion Resistance, and Immobilization Capabilities. *ACS Applied Materials & Interfaces* 2019;11(17):15709-17.
- [56] Ucar S, Karagoz S, Ozkan AR, Yanik J. Evaluation of two different scrap tires as hydrocarbon source by pyrolysis. *Fuel* 2005;84(14):1884-92.
- [57] Williams PT, Bottrill RP. Sulfur-polycyclic aromatic hydrocarbons in tyre pyrolysis oil. *Fuel* 1995;74(5):736-42.
- [58] K k MV, Varfolomeev MA, Nurgaliev DK. Crude oil characterization using TGA-DTA, TGA-FTIR and TGA-MS techniques. *Journal of Petroleum Science and Engineering* 2017;154:537-42.
- [59] Garc a-Guti rrez JL, Fuentes GA, Hern ndez-Ter n ME, Garcia P, Murrieta-Guevara F, Jim nez-Cruz F. Ultra-deep oxidative desulfurization of diesel fuel by the Mo/Al<sub>2</sub>O<sub>3</sub>-H<sub>2</sub>O<sub>2</sub> system: The effect of system parameters on catalytic activity. *Applied Catalysis A: General* 2008;334(1-2):366-73.
- [60] Hossain MN, Choi MK, Park HC, Choi HS. Purifying of Waste Tire Pyrolysis Oil Using an S-ZrO<sub>2</sub>/SBA-15-H<sub>2</sub>O<sub>2</sub> Catalytic Oxidation Method. *Catalysts* 2020;10(4):368.